Building a better cell trap: Applying Lagrangian modeling to the design of microfluidic devices for cell biology

Min-Cheol Kim, Zhanhui Wang, Raymond H. Lam, and Todd Thorsen

Citation: J. Appl. Phys. **103**, 044701 (2008); doi: 10.1063/1.2840059
View online: http://dx.doi.org/10.1063/1.2840059
View Table of Contents: http://jap.aip.org/resource/1/JAPIAU/v103/i4
Published by the American Institute of Physics.

Building a better cell trap: Applying Lagrangian modeling to the design of microfluidic devices for cell biology

Min-Cheol Kim,[1] Zhanhui Wang,[1] Raymond H. W. Lam,[1] and Todd Thorsen[1,a)]
[1]*Department of Mechanical Engineering, Massachusetts Institute of Technology, Cambridge, Massachusetts 02139, USA*

(Received 19 April 2007; accepted 3 December 2007; published online 19 February 2008)

In this report, we show how computational fluid dynamics can be applied to the design of efficient hydrodynamic cell traps in microfluidic devices. Modeled hydrodynamic trap designs included a large, multiple-aperture "C-type" sieve for trapping hundreds of cells, flat single-aperture arrays for single cells, and "U-type" hydrodynamic structures with one or two apertures to confine small clusters of cells (~10–15 cells per trap). Using 3T3 cells as a model system, the motion of each individual cell was calculated using a one-way coupled Lagrangian method. The cell was assumed to be a solid sphere, and interactions with other cells were only considered when a cell sedimented in the trap. The ordinary differential equations were solved along the cell trajectory for the three components of the velocity and location vector by using the Rosenbrock method based on an adaptive time-stepping technique. Validation of the predictive value of modeling, using 3T3 cells flowed through microfluidic devices containing "U-type sieves" under the simulation flow parameters, showed excellent agreement between experiment and simulation with respect to cell number per trap and the uniformity of cell distribution within individual microchambers. For applications such as on-chip cell culture or high-throughput screening of cell populations within a lab-on-a-chip environment, Lagrangian simulations have the potential to greatly simplify the design process. © *2008 American Institute of Physics*. [DOI: 10.1063/1.2840059]

INTRODUCTION

Microfluidic devices, often referred to by the name "lab-on-a-chip," provide a unique environment to study single cells or small populations of cells in ultralow media volumes. Consequently, there has been a growing interest within the research community in the design of microfluidic devices for immobilizing cells,[1–15] incorporating physical methods, including dielectrophoresis[5] and optical traps,[12] as well microstructures such as physical weirs[9–11] and active valving elements,[13,14] to isolate cells of interest. While microfluidic devices have often been promoted as tools for high-throughput screening, with the potential to multiplex molecular assays while reducing reagent consumption,[14] the miniaturization of cell culture-based platforms presents unique challenges. In reducing the cell culture media volume from milliliters to the nanoliters encountered in microfluidic devices, careful control protocols must be developed to create a balanced environment to maximize cell viability and proliferation, providing nutrients while removing waste products. Consequently, controlling cell seeding density in culture-based microdevices is of critical importance, as single cell isolates lack critical biochemical stimulants secreted by neighbor cells, while, in cultures that are too dense, lack of resources (nutrients and oxygen) promote cell death via necrosis and apoptosis.[16–18]

From a design perspective, achieving a uniform trapping within a device can be quite challenging, as the flow fields within microchannels are continually changing during the cell loading process. Many passive devices have been developed with microfabricated solid supports that function as cell traps.[9–11] Wilding *et al.* designed 3.5 μm feature-sized "weir-type" filters formed by an etched dam spanning a flow chamber to isolate white blood cells from whole blood.[19] Subsequently, many weir-type or damming filters for multicell trapping have been reported in microfluidic devices, including U-shaped microstructures[3,4,9,15] and C-shaped rings with microsieves.[2]

In this study, we introduce dynamic cell simulations, which are based on the Lagragian approach, to track the trapping behavior of individual cells when confronted with arrays of sieve traps within microfluidic device chambers. Several sieve geometries are analyzed, with the validation of the simulation carried out experimentally using polydimethylsiloxane (PDMS)-based devices containing an array of U-shaped sieve traps designed to capture ~10–15 cells per trap. The cell trapping microfluidic devices were designed to satisfy two conditions: rapid isolation of cells from the bulk solution and uniform distribution of cells trapped per sieve across the individual chambers. While the work of many groups designing microfluidic devices for cell-biology-based applications have focused on single cells,[4–6,8–11] prolonged on-chip culture of single cells remains a challenge. For applications such as cell cytotoxicity monitoring[20] or gene expression analysis,[13] the health of the culture is critical to obtain statistically meaningful results.

METHODS

Geometrical modeling

To generate the computational model in the microfluidic system, we first converted the two-dimensional (2D) pattern of a microchannel, which was drawn using AUTOCAD soft-

a)Author to whom correspondence should be addressed. Electronic mail: thorsen@mit.edu.

ware, into a three-dimensional (3D) geometric structure. This structure was made in a stereolithography (STL) file format and extruded in the direction of channel height. Then, the surface geometry of the STL file was imported into a commercial automeshing software package (PRO-AM, CD-adpaco).[21] Further refinements to the STL file, including surface triangulation and optimization for computational cell shapes, were carried out to enable the modeling of particle interactions with the inner surfaces of microchannels. The final computational mesh consisted of $\sim 8 \times 10^5$ elements.

Fluid modeling

Computational fluid dynamics (CFD) simulations were carried out using a commercial CFD tool (STAR-CD Version 3.15a, CD-adpaco), which is based on the finite volume method. For the working fluid, aqueous solution ($\rho_f = 997.5\ \mathrm{kg/m^3}$) was selected to emulate buffered ion solutions used in microdevices. Momentum equations and the continuity equation were solved using the semi implicit method for pressure linked equation (SIMPLE) algorithm with a tolerance of 0.001. The SIMPLE algorithm was used for the calculation of steady problems with one predictor stage and one corrector stage iteratively. Algebraic multigrid (AMG) was applied as a linear algebraic equation solver, as it operates independently of the underlying geometries.[22] Numerically, UD (upwind scheme, first order of accuracy) was implemented for spatial discretization with residual tolerances of each velocity component and pressures of 0.1 and 0.05, respectively. At the chamber inlet, a flat velocity profile was imposed at a uniform flow rate of 1 μl/min and a constant pressure ($P = P_{\mathrm{atm}}$) boundary condition was imposed at the outlet.

Cell modeling

The one-way coupled Lagrangian approach for the precomputed Newtonian flow fields was applied to calculate the transient motion of individual cells, which includes the spatial interpolation of the flow velocity at the individual cell positions. Each cell was modeled as a sphere (diameter of 10 μm) in aqueous solution. The equation of motion for the cells included the Stokes drag, the pressure gradient, diffusive and gravitational forces, and a spring force to model elastic collisions between individual cells.[23] The resulting cell motion equations for particle velocity ($\mathbf{u}_p^*$) and location ($\mathbf{x}_p^*$) are expressed as

$$\frac{d\mathbf{u}_p^*}{dt} = \frac{(\mathbf{u}_f - \mathbf{u}_p^*)}{\tau_p} + \alpha \frac{d\mathbf{u}_f}{dt} + \frac{\mathbf{F}_r}{m_p} + (1-\alpha)\mathbf{g} + \frac{\mathbf{F}_s}{m_p}, \tag{1}$$

$$\frac{d\mathbf{x}_p^*}{dt} = \mathbf{u}_p^*, \tag{2}$$

where $\tau_p (= \rho_p d_p^2 / 18\eta_f)$ is the particle response time to changes in the flow field, η_f is the dynamic viscosity of the fluid ($\eta_f = 8.88 \times 10^{-3}\ \mathrm{kg\ m^{-1}\ s^{-1}}$), d_p is the particle diameter (10 μm), and α is the fluid/particle density ratio ($\rho_f = 997.5\ \mathrm{kg\ m^{-3}}$ and $\rho_p = 1040\ \mathrm{kg\ m^{-3}}$). Elastic collisions between cells were modeled using an effective spring force $\mathbf{F}_s$ represented by

$$\mathbf{F}_s = \begin{cases} 0 & \text{if } d_{ij} > d_p \\ \sum_{i=1}^{N} k_p (d_p - d_{ij}) \hat{n}_{ij} & \text{else,} \end{cases} \tag{3}$$

where k_p is the effective stiffness constant of the cell based on a transformed cell line ($3.2 \times 10^{-4}\ \mathrm{N/m}$),[23] d_{ij} is the distance between the centers of cells i and j, $\hat{n}_{ij}$ is normal vector between cells i and j, and N is the total number of seeded cells in the computational domain. $\mathbf{F}_r$ represents the Brownian random force, which is induced by collisions between microparticles and fluid molecules and is based on the Monte Carlo method for mimicking the random walk of particles. For the three-dimensional case, the random walk algorithm is expressed as

$$\Delta x = \sqrt{4Ddt}\cos(\theta)\sin(\phi),$$

$$\Delta y = \sqrt{4Ddt}\sin(\theta)\sin(\phi),$$

$$\Delta z = \sqrt{4Ddt}\cos(\phi), \tag{4}$$

where $D (= k_B T / 3\pi d_p \eta)$ is the Einstein relation for the diffusion of particles, θ=random $(0, 2\pi)$, and ϕ=random $(0, \pi/2)$.

To compensate for interactions between cells and solid wall boundaries within the device, a particle rolling (PR) model was employed as an additional constraint. The PR model has been previously validated in work comparing numerical simulations with experimental data in the analysis of normalized platelet density in a stagnation point flow chamber and normalized monocyte distribution in a stenotic tube.[24] The PR model decomposes the particle velocity vector into normal and tangential components, subsequently forcing the normal component to zero. When the cell is located in the near-wall region, where distance from the center of the particle to the wall surface (h_p) is less than cell's radius (r_p), i.e., the cell contacts or collides with the surface, the inward vertical cell velocity (U_h) is nonzero and the cell intersects with the computational domain. To offset the cell-wall interaction, preventing cells from penetrating the solid boundaries defined in the CFD simulation, a geometric correction factor (δ_h) is applied that resets the cell position vector to simulate deflection. U_h and δ_h are defined as follows:

$$U_h = \begin{cases} |\mathbf{u}_p^* \cdot \hat{n}_w| & \text{if } \mathbf{u}_p^* \cdot \hat{n}_w < 0 \\ 0 & \text{else,} \end{cases} \tag{5}$$

$$\delta_h = \begin{cases} 1.5(r_p - h_p) & \text{if } h_p < r_p \\ 0 & \text{else,} \end{cases} \tag{6}$$

where $\mathbf{u}_p^*$ is the predicted particle velocity solved from Eqs. (1) and (2) and $\hat{n}_w$ is an inward pointing normal vector of the wall surface. Finally, the velocity and position vectors in the near-wall region were corrected as

$$\mathbf{u}_p = \mathbf{u}_p^* - U_h \hat{n}_w, \tag{7}$$

$$\mathbf{x}_p = \mathbf{x}_p^* + \delta_h \hat{n}_w, \tag{8}$$

where $\mathbf{x}_p^*$ is the predicted particle position vector.

Each cell trajectory was obtained by integrating Eqs. (1) and (2) under given initial conditions, subject to the constraints imposed in Eqs. (5) and (6). The initial cell velocity was interpolated using the fluid velocity at the initial cell's seeding location. The cell seeding concentration was set at either 10^6/ml (initial qualitative model) or 5×10^6/ml at a bulk flow rate of 1.0 μl/min. A fourth order Rosenbrock method based on an adaptive time-stepping technique was utilized as the integration method, as it exhibited a more reliable data trend without divergence than the Runge–Kutta method.[25] The experimental results of hardened red blood cells flowing through an annular expansion channel were used to validate the cell trajectory code.[24,26]

A program written in C++ (Microsoft), which we refer to as the "lab chip designer" (LCD), was used to model the Lagrangian cell dynamics within the simulated microchambers. As the Lagrangian coupling is only one way, the motion of each individual cell is dependent on the underlying flow field, while the flow field only depends on the device geometry (i.e., the presence of cells does not alter the flow field). The LCD program performs three procedures (reading input data, solving of cell motion equations, and postprocessing of output data) to generate the cell trajectories in the microchamber. Input data are categorized into two types: 3D geometrical information mapping the physical features of the device and CFD results of the flow fields. After importing the flow and boundary data, simulated cells were introduced into the flow field via statistically random uniform seeding across the chamber inlet. After seeding, each cell flowed through the chamber, interacting with the fluid and solid elements (walls and other cells) under the constraints developed in the previous section. At each time step, the LCD program updates the position of individual cells within the computational domain. Once the cells were deposited in the sieves, final location vectors of those cells were sequentially recorded. To visualize the cell distribution versus time, data were exported to generate frame stills using a commercial plot software package (TECPLOT 10).

Device fabrication

Microfluidic cell trapping devices containing multiple U-shaped sieves were fabricated in PDMS (Sylgard 184, Dow Corning) using established soft lithography molding techniques.[27] To fabricate the device mold, AZXT50 positive photoresist (AZ Electronic Materials USA Corp.) was patterned onto a silicon wafer using a high-resolution transparency (3550 dots/in., MikaColor) as a mask to define the microchannel features. After development, the molds were hard baked on a hot plate at 150 °C for 1 min to toughen the resist and extend the mold lifetime. After the postbake, the molds were silanized [trichlorotrimethylsilane (Aldrich)] to promote mold release during the PDMS casting process. To create the elastomeric devices, PDMS was mixed in a ratio of 10:1 part A:B, poured onto the mold to a thickness of ~5 mm, and baked at 80 °C for 30 min. After baking, the PDMS device was peeled off the mold and inlet and outlet holes were punched through the device with a 23 gauge luer stub (BD Biosciences). The punched holes were subsequently cleaned with isopropanol to remove debris and dried under a nitrogen stream. After cleaning, oxygen plasma was used to bond the PDMS devices (channel side down) to a glass slide (150 mTorr, 50 W, 20 s). In the final assembled devices, the flow channels at the inlet and outlet are 40 μm (h) $\times$ 100 μm (w), connecting to a circular chamber at each channel intersection (diameter of 400 μm). Each circular chamber contains eight to nine PDMS U-shaped cell sieves, depending on the array design. Each sieve is semicircular, 80 μm (d), 20 μm (w), and 40 μm (h), with two apertures (8 μm).

Cell culture and microfluidic trapping

The BALB/3T3 cell line (Advanced Tissue Culture Collection) used in the experimental validation of microfluidic cell trapping was maintained in Dulbecco modified eagle medium supplemented with 10% fetal bovine serum and cultured at 37 °C/5% CO_2 in a humidified incubator. Once the cells were confluent, they were trypsinized (0.25% in EDTA, Sigma) and passaged at a 1:5 subculture ratio. In preparation for trapping, 10 ml of passaged cells was transferred to a 50 ml conical tube, gently centrifuged (2000 rpm, 5 min), and resuspended in 5 ml 1× phosphate-buffered saline (PBS), pH 7.4. To adjust the culture density to 5×10^6/ml (equivalent to the simulation seeding density), a haemocytometer was used to count the cells and the cells were diluted appropriately using 1× PBS. Cell loading was achieved using a syringe pump (Harvard Apparatus) to flow the cells though the microfluidic devices at a volumetric flow rate of 1 μl/min for a period of 90 s. After loading, the cells in the traps within the chambers were counted using an inverted light microscope [Nikon TE2000-U, 10× plan objective, numerical aperature (NA) 0.25].

RESULTS AND DISCUSSION

In our first set of qualitative simulations, we looked at several sieve-based trapping designs, including semicircular "C-shaped" sieves with 13 apertures, flat sieves with a single aperture, and U-shaped sieves with one aperture (Fig. 1). Each simulation was carried out at a volumetric flow rate of 1.0 μl/min and a cell seeding density of 1×10^6/ml run for a total of 60 s.

Inspection of the results for the C-shaped sieve [Fig. 1(a)] shows pronounced aggregation of the cells in the downstream section of the trap. Large cell aggregates are particularly unfavorable for microscale cell culture, as they can quickly exhaust the local nutrients and reduce oxygenation efficiency, stressing the culture to the point of cell death by necrosis or apoptosis. The core of large cell aggregates (>100 μm diameter) is particularly vulnerable to cell death, where the dominant mechanism of metabolite and gas exchange is diffusion.[28] This effect can be mitigated to some extent by increasing the media flow rate through the microchamber, increasing the perfusion rate of core cells, but ex-

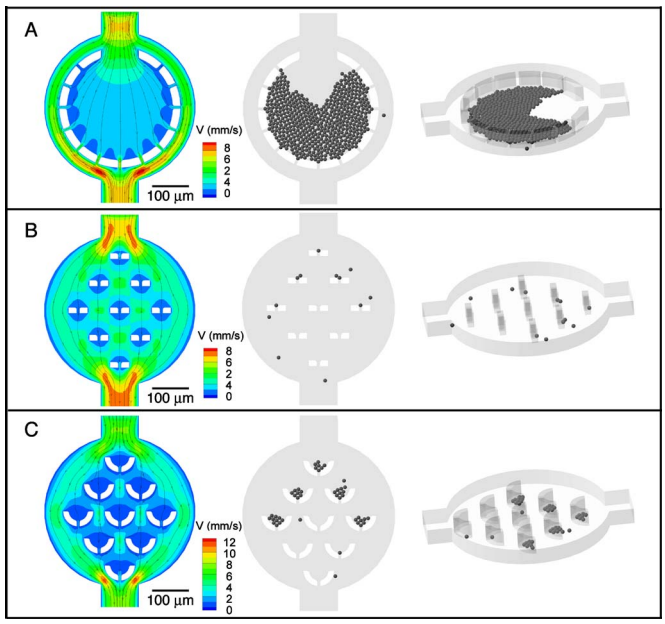

FIG. 1. (Color online) Streamlines and cell traps in simulations of different types of cell trapping chambers: (A) is the "C-shaped" sieve, (B) is the "flat-type" sieve, and (C) is the "U-type" sieve with "one aperture." Left panel shows fluid velocity magnitude contours and selected streamlines and right panel shows the final state of trapped cells as results of simulations in the three different chambers.

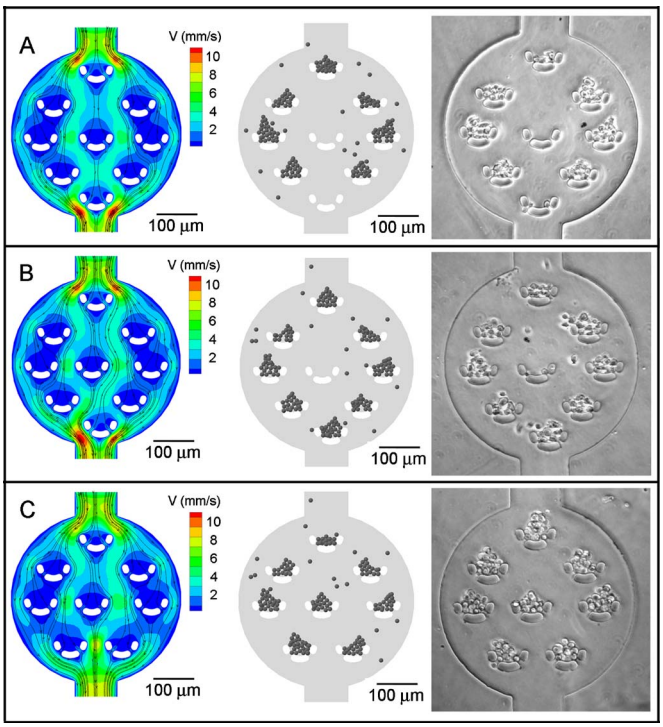

FIG. 2. (Color online) Simulation vs experimental loading of microchambers containing different arrangements of two-aperture U-shaped trapping sieves: (A) is "U-type" sieve A, (B) is U-type sieve B, and (C) is "U-type" sieve C with dual aperture. Left panel shows fluid velocity magnitude contours and selected streamlines, middle panel shows the final state of trapped cells as results of each simulation in the three different chambers, and right panel shows the final state of trapped cells as results of each experiment in the three different chambers.

cessively high flow rates also work against the overall culture health by removing secreted cell factors that promote growth and proliferation.

The flat-type sieve [Fig. 1(b)] and the initial U-type sieve arrays (Fig. 1(c)), consist of an array of nine sieves arranged in a symmetric diamond-shaped pattern. Under simulated conditions, sieves closer to the chamber entrances captured cells well for both geometries, while the downstream sieves remained empty. The relative loading efficiency of the simulated traps can be explained in terms of the flow streamlines and the symmetry of the trap arrays. Streamlines close to the solid boundaries ($<$ radius of an individual cell) are inaccessible to cells. For symmetrical sieve arrays, unique streamlines bisect the center of multiple apertures. As there is only a one-way coupling between the fluid and cell simulations, the presence of trapped cells has no effect on the underlying flow field. Consequently, cells flowing on these bisecting streamlines are excluded from all traps except the one closest to the microchamber inlet. Increasing the loading efficiency of the sieves can be achieved by breaking the symmetry. An excellent example of asymmetric flat-plate single-cell hydrodynamic trap arrays has been recently demonstrated by Di Carlo *et al.*, utilizing high-density PDMS microfluidic arrays with a trapping efficiency of $>50\%$.[11]

To demonstrate the predictive value of the model against an experimental platform, a comparison was made between the simulated cell loading of a U-shaped sieve array (with two 8 μm apertures/sieve) and the experimental loading of PDMS microfluidic array devices with 3T3 cells (Fig. 2). Both simulation and experiments used a cell concentration of 5×10^6/ml, a bulk flow rate of 1 μl/min, and a loading time of 90 s. The designs shown in Figs. 2(a) and 2(b) have nine U-shaped sieves per microchamber. In the first design [case A, Fig. 2(a)], the nine sieves are arranged symmetrically across the chamber. Cells flowed though this sieve arrangement trap cells in the peripheral sieves near the chamber walls, leaving the downstream central sieves empty. By shifting the positions of the center sieve and the bottom sieve nearest to the chamber outlet by 10 μm to the left and right, respectively, the symmetry of the traps within the array was broken, promoting cell capture in all sieves with the exception of the center sieve [case B, Fig. 2(b)]. In the final U-shaped trap array [case C, Fig. 2(c)], the trap nearest to the chamber outlet was removed, the position of the traps in the third row was restored to the configuration in case A, and the top trap nearest to the inlet was shifted down by 10 μm. The simulation result showed efficient capture of a small population of cells in each sieve. Good correlation was observed between simulated results and experimental cell trapping of 3T3 cells in the PDMS microfluidic device with respect to filling of the individual sieves and cell number per sieve. For the collection of experimental data, trapped cells in the sieve arrays of 100 microchambers were counted using an inverted light microscope (Nikon TE2000-U, 10$\times$ plan objective, NA 0.25) for each case. For case A, the number of trapped cells per sieve predicted by theory (16.6 ± 1.0 cells per sieve) is comparable to 11.7 ± 5.6 obtained experimentally. For cases B and C, the theoretical versus experimental values are 19.8 ± 0.8 vs 13.9 ± 4.2 and 21.2 ± 1.2 vs 15.0 ± 3.9 cells per sieve, respectively. The higher standard deviation of the ex-

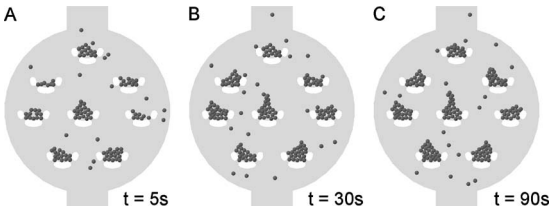

FIG. 3. Simulation of cell loading in dual aperture U-type sieves (case C) at discrete time steps.

perimental results is not surprising, as cell-cell clumping is quite common, even in well-suspended cultures, leading to the deposition of small cell aggregates in the sieves.

To investigate the dynamics of the cell trapping process, the simulated loading of the individual trapping arrays and sieve conformations was analyzed at discrete time steps. A simulated time step analysis for case C is shown in Fig. 3. Analysis of the figure reveals that the filling of the traps at the prescribed flow rate and cell concentration (1 μl/min, 5×10^6 cells/ml) occurs quite rapidly. By 30 s, most of the traps are fully occupied, with few cells added between 30 and 90 s. A plot of cell number per sieve as a function of time over a period of 2 min for all three cases (A, B, and C) is shown in Fig. 4. From the figure, the trapping rate is quadratic with respect to time for a period of ~15 s, after which very few cells are deposited in the traps for extended loading periods. As the U-shaped sieves approach their maximum cell retention capacity ($t>60$ s), elastic cell-cell collisions force impinging cells into regions of the flow field that sweep them toward the microchamber outlet.

Within the last decade, many groups have applied CFD to the modeling of the migration of cells in milli- and microconduits. Research efforts in this area include the modeling of red blood cells in capillaries,[29–32] circulatory flow through stents,[33,34] and tissue perfusion.[35,36] Glicklis *et al.* recently coupled the Navier–Stokes equations to protein molecular dynamics to study cell-cell interactions between red blood cells in microcapillaries, considering attractive/repulsive forces such as membrane charge density coupled with hydrodynamic forces imposed by the flow field.[28] However, the analysis of cell migration hydrodynamics in microfluidic devices has been limited. Modeling the efficacy of cell separation using weirs considering only a 2D flow field, neglecting particle interaction, has been carried out by Panaro *et al.*[37] Analytical and computational models have also been developed for the capture of cells in microdevices using dielectrophoresis, considering effects such as cell velocity coupled with field strength and electrode geometry.[38,39]D. D. Carlo *et al.* developed a microfluidic cell trapping model confined to single structures, considering only the viscous components of flow.[19] Our model differs from previous cell modeling work in microfluidic devices in that we consider both viscous and inertial terms in the Navier–Stokes equation to account for both the migration of cells through the microchambers and their deceleration as they become confined on the microsieves. With the ability to interface the particle dynamics with the fluid mechanics within the underlying device, the LCD program is a good computer-aided design (CAD) tool for microfluidic engineering.

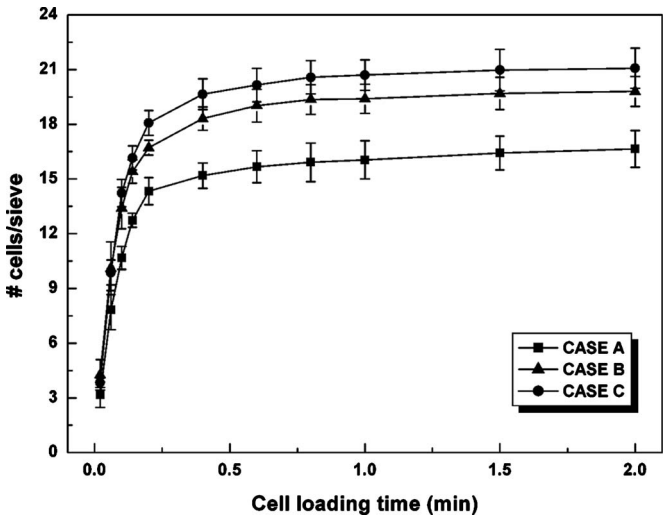

FIG. 4. Simulated trapped cell number vs time for dual aperture U-type sieves (cases A, B, and C).

CONCLUSIONS

In this manuscript, we report on the development of a simulation method to model the trapping of cells in sieve structures within a microfluidic device, coupled with experimental validation. The model couples the flow field properties within a microchamber with a Lagrangian approach to particle tracking. Good agreement was observed between simulation and experiment, both with respect to the cell distribution across the sieves and the number of trapped cells per sieve. Presently, the LCD program is limited by one-way coupling (the flow field influences the particle physics, but not vice versa). A potential improvement to the model, while computationally intensive, would be to create an iterative feedback loop to analyze the effects of particle position on flow field.

ACKNOWLEDGMENTS

This work was supported in part by a Korean Research Foundation Grant funded by the Korean Government (MOE-HRD), KRF-2006-D00019.

[1]A. Khademhosseini, J. Yeh, G. Eng, J. Karp, H. Kaji, J. Borenstein, O. C. Farokhzad, and R. Langer, Lab Chip **5**, 1380 (2005).
[2]P. J. Lee, P. J. Hung, V. M. Rao, and L. P. Lee, Biotechnol. Bioeng. **94**, 5 (2006).
[3]A. R. Wheeler, W. R. Throndset, R. J. Whelan, A. M. Leach, R. N. Zare, Y. H. Liao, K. Farrell, I. D. Manger, and A. Daridon, Anal. Chem. **75**, 3581 (2003).
[4]M. S. Yang, C. W. Li, and J. Yang, Anal. Chem. **74**, 3991 (2002).
[5]J. Voldman, M. L. Gray, M. Toner, and M. A. Schmidt, Anal. Chem. **74**, 3984 (2002).
[6]X. Y. Peng and P. C. H. Li, Anal. Chem. **76**, 5273 (2004).
[7]U. Seger, S. Gawad, R. Johann, A. Bertsch, and P. Renaud, Lab Chip **4**, 148 (2004).
[8]H. K. Wu, A. Wheeler, and R. N. Zare, Proc. Natl. Acad. Sci. U.S.A. **101**, 12809 (2004).
[9]P. C. H. Li, L. de Camprieu, J. Cai, and M. Sangar, Lab Chip **4**, 174 (2004).
[10]X. J. Li and P. C. H. Li, Anal. Chem. **77**, 4315 (2005).
[11]D. Di Carlo, N. Aghdam, and L. P. Lee, Anal. Chem. **78**, 4925 (2006).
[12]K. C. Neuman, E. H. Chadd, G. F. Liou, K. Bergman, and S. M. Block,

Biophys. J. **77**, 2856 (1999).
[13]K. R. King, S. Wang, D. Irimia, J. Jayaraman, M. Toner, and M. L. Yarmush, Lab Chip **7**, 77 (2007).
[14]T. Thorsen, S. J. Maerkl, and S. R. Quake, Science **298**, 580 (2002).
[15]D. D. Carlo, L. Y. Wu, and L. P. Lee, Lab Chip **6**, 1445 (2006).
[16]S. N. Bhatia, U. J. Balis, M. L. Yarmush, and M. Toner, Biotechnol. Prog. **14**, 378 (1998).
[17]J. El-Ali, P. K. Sorger, and K. F. Jensen, Nature (London) **442**, 403 (2006).
[18]G. M. Walker, H. C. Zeringue, and D. J. Beebe, Lab Chip **4**, 91 (2004).
[19]P. Wilding, L. J. Kricka, J. Cheng, G. Hvichia, M. A. Shoffner, and P. Fortina, Anal. Biochem. **257**, 95 (1998).
[20]Z. Wang, M.-C. Kim, M. Marquez, and T. Thorsen, Lab Chip **7**, 740 (2007).
[21]STAR-CD, Version 3.24, methodology CD-adapco, 2005.
[22]Tutorials PRO-STAR with automesh generation, Version 3.24, CD-adapco, 2005.
[23]W. A. Lam, M. J. Rosenbluth, and D. A. Fletcher, Blood **109**, 3505 (2007).
[24]M.-C. Kim, J. H. Nam, and C.-S. Lee, Ann. Biomed. Eng. **34**, 958 (2006).
[25]W. H. Press, S. A. Teukolsky, W. T. Vetterling, and B. P. Flannery, *Numerical Recipes in C* (Cambridge University Press, Cambridge, 1992) Chap. 16, p. 734.
[26]T. Karino and H. Goldsmith, Philos. Trans. R. Soc. London, Ser. B **279**, 413 (1977).
[27]Y. Xia and G. M. Whitesides, Annu. Rev. Mater. Sci. **28**, 153 (1998).
[28]R. Glicklis, J. C. Merchuk, and S. Cohen, Biotechnol. Bioeng. **86**, 672 (2004).
[29]Y. Liu, L. Zhang, W. Wang, and W. K. Liu, Int. J. Numer. Methods Fluids **46**, 1237 (2007).
[30]W. Dzwinel, K. Boryczko, and D. A. Yuen, J. Colloid Interface Sci. **258**, 163 (2003).
[31]Y. Q. Huang, C. M. Doerschuk, and R. D. Kamm, J. Appl. Physiol. **90**, 545 (2001).
[32]K. S. Burrowes, M. H. Tawhai, and P. J. Hunter, Ann. Biomed. Eng. **32**, 585 (2004).
[33]A. O. Frank, P. W. Walsh, and J. E. Moore, Artif. Organs **26**, 614 (2002).
[34]J. L. Berry, A. Santmarina, J. E. Moore, S. Roychowdhury, and W. D. Routh, Ann. Biomed. Eng. **28**, 386 (2000).
[35]R. A. Peattie and R. J. Fischer, Adv. Biochem. Eng./Biotechnol. **103**, 75 (2007).
[36]S. L. Xu, D. C. Li, Y. Z. Xie, J. X. Lu, B. H. Lu., Z. A. Zhu, T. T. Tang, K. R. Dai, and Z. Wang, Progress Biochem. Biophys. **33**, 895 (2006).
[37]N. J. Panaro, X. J. Lou, P. Fortina, L. J. Kricka, and P. Wilding, Biomol. Eng. **21**, 157 (2004).
[38]D. R. Albrecht, R. L. Sah, and S. N. Bhatia, Biophys. J. **87**, 2131 (2004).
[39]T. R. Schnelle, R. Hagedorn, G. Fuhr, S. Fiedler, and T. Muller, Biochim. Biophys. Acta **1157**, 127 (1993).